Portable Roadside Sensors for Vehicle Counting, Classification, and Speed Measurement

Saber Taghvaeeyan and Rajesh Rajamani

***Abstract*—This paper focuses on the development of a portable roadside magnetic sensor system for vehicle counting, classification, and speed measurement. The sensor system consists of wireless anisotropic magnetic devices that do not require to be embedded in the roadway—the devices are placed next to the roadway and measure traffic in the immediately adjacent lane. An algorithm based on a magnetic field model is proposed to make the system robust to the errors created by larger vehicles driving in the nonadjacent lane. These false calls cause an 8% error if uncorrected. The use of the proposed algorithm reduces this error to only 1%. Speed measurement is based on the calculation of the cross correlation between longitudinally spaced sensors. Fast computation of the cross correlation is enabled by using frequency-domain signal processing techniques. An algorithm for automatically correcting for any small misalignment of the sensors is utilized. A high-accuracy differential Global Positioning System is used as a reference to measure vehicle speeds to evaluate the accuracy of the speed measurement from the new sensor system. The results show that the maximum error of the speed estimates is less than 2.5% over the entire range of 5–27 m/s (11–60 mi/h). Vehicle classification is done based on the magnetic length and an estimate of the average vertical magnetic height of the vehicle. Vehicle length is estimated from the product of occupancy and estimated speed. The average vertical magnetic height is estimated using two magnetic sensors that are vertically spaced by 0.25 m. Finally, it is shown that the sensor system can be used to reliably count the number of right turns at an intersection, with an accuracy of 95%. The developed sensor system is compact, portable, wireless, and inexpensive. Data are presented from a large number of vehicles on a regular busy urban road in the Twin Cities, MN, USA.**

***Index Terms*—Magnetic sensors, portable traffic sensor, roadside traffic sensor, vehicle classification, vehicle detection, vehicle speed measurement.**

I. Introduction

THIS paper describes a portable sensing system that can be placed adjacent to a road and can be used for vehicle counting, vehicle classification, and vehicle speed measurements. The proposed system can make these traffic measurements reliably for traffic in the lane adjacent to the sensors. The developed signal processing algorithms enable the sensor to be robust to the presence of traffic in other lanes of the road.

The sensor consists of magnetoresistive devices that measure the magnetic field. Signal processing algorithms based on an analysis of the magnetic field around a car are used to enable the sensor estimates. The developed sensing system is compact, portable, wireless, and inexpensive (with an expected cost on the order of $50).

Inductive loop detectors (ILDs) are a widespread technology used by many transportation agencies for vehicle detection and measurement of traffic flow rates. Single inductive loops, by themselves, do not measure individual vehicle speed.

Vehicle classification into predefined classes such as cars, trucks, and tractor trailers typically requires measuring the size or length of a vehicle and/or counting the number of axles of the vehicle. A vehicle classification model based on feature extraction from piecewise slope rate values in single-loop inductive signature data was pursued in [1] and classified vehicles into 15 classes. However, the accuracy rate is not 100% and can vary from 40% to 100%, depending on the amount of "problematic" data present in the sensor readings and the class of vehicle under consideration.

Vehicle detection and classification based on feature extraction from camera systems have been developed by many researchers [2], [3]. The research in [3] presented model-based and fuzzy-logic approaches to improve the reliability of such systems. An evaluation of three commercial camera-based vehicle detection systems is presented in [4] under adverse weather conditions of snow, fog, and rain. The results therein show that the performance of such systems deteriorates under adverse weather, particularly under snow conditions in both daytime and nighttime. Increases in false activations by up to 90% and in missed calls by up to 50% were shown to occur in adverse weather.

Magnetic sensors and anisotropic magnetoresistive (AMR) sensors have also been evaluated for vehicle classification by some research groups [5]–[11]. The main limitation of these works is their inability to distinguish between sedans versus sport utility vehicles (SUVs), pickups, and vans. Mostly, these two classes are combined, or poor classification rates are obtained when these are considered as individual classes. Furthermore, the magnetic sensors that have been evaluated are based on devices that were directly embedded in the roadway lanes.

Unlike inductive loops and magnetic sensors that have been evaluated, the sensing system proposed in this paper does not require devices to be embedded in the roadway. Instead, it utilizes sensors that are placed on the side of the road, and hence, there is no need to stop the traffic for their installation. In addition, the sensor system used is very compact and wireless and can provide very high accuracies in vehicle detection, speed measurement, and classification.

Manuscript received March 25, 2013; revised May 22, 2013; accepted July 2, 2013. Date of publication September 25, 2013; date of current version January 31, 2014. This work was supported in part by the ITS Institute, University of Minnesota. The Associate Editor for this paper was F. Zhu.

The authors are with the University of Minnesota, Twin Cities, Minneapolis, MN 55455 USA (e-mail: rajamani@me.umn.edu).

Color versions of one or more of the figures in this paper are available online at http://ieeexplore.ieee.org.

Digital Object Identifier 10.1109/TITS.2013.2273876

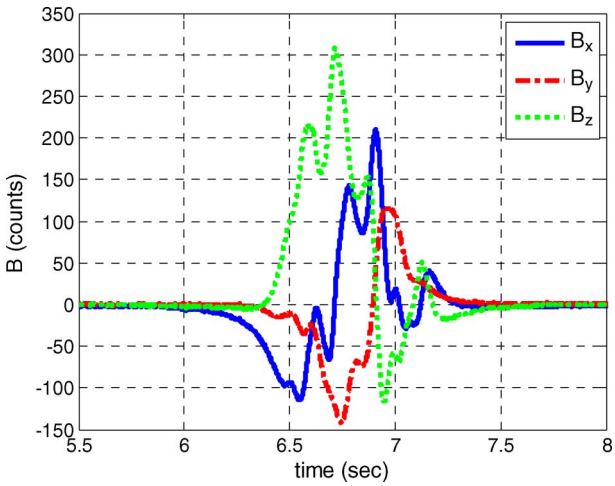

Fig. 1. Magnetic field readings for a Ford Ranger from a magnetic sensor embedded in the road.

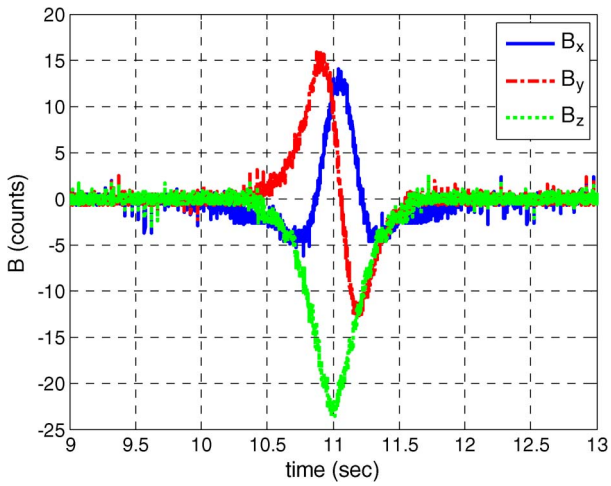

Fig. 2. Magnetic field readings for a Ford Ranger from a magnetic sensor adjacent to the road.

This paper is organized as follows. In Section II, the signal strength and sensing system configuration is discussed. In Section III, the detection performance of the system is presented. The method that was developed to make the system robust to traffic in the nonadjacent lane is described in Section IV. In Section V, the speed estimation method is described. Vehicle classification is discussed in Section VI. A method of counting the number of vehicles that make a right turn at an intersection is discussed in Section VII. Conclusions are presented in Section VIII.

II. Signal Strength and Sensing System Configuration

An AMR sensor has a silicon chip with a thick coating of piezoresistive nickel–iron. The presence of an automobile in close range causes a change in magnetic field, which changes the resistance of the nickel–iron layer. The HMC2003 three-axis magnetic sensor boards from Honeywell are utilized for the system developed in this paper. Each sensor board contains core HMC100x AMR sensing chips, which cost about $10.

First, magnetic field readings were obtained from a magnetic sensor that was embedded on top of the road surface at the center of a lane and compared with the magnetic field readings when the sensor was placed adjacent to the road. Fig. 1 shows the magnetic field readings of the x-, y-, and z-axes, with the sensor placed at the center of the road lane. Here, the x-axis is along the longitudinal direction of travel of the vehicles, the y-axis is perpendicular to the direction of travel of the vehicles, and the z-axis is perpendicular to the road surface and upward. Fig. 2 shows magnetic field readings when the magnetic sensor was placed adjacent to the road at a height of about 0.6 m. It is clearly shown that the magnetic field readings due to the vehicle are ten times stronger when the sensor was placed on the road. The vehicle that was used for these two tests was a Ford Ranger pickup truck.

It is also shown in Figs. 1 and 2 that, when the sensors are placed on the side of the road, the signals are more uniform compared to the case that the sensors are on the road. The main reason is that, with the sensors on the road, many different ferromagnetic parts underneath the vehicle will pass over the sensors at close proximity and create extra fluctuations in the signal. Because the original signal levels are low when the sensors are placed on the side of the road, it is necessary to use higher amplification to get a better signal-to-noise ratio (SNR). Hence, the sensor signals were amplified using instrumentation amplifiers, with cutoff frequencies set to 100 Hz to reduce the noise level.

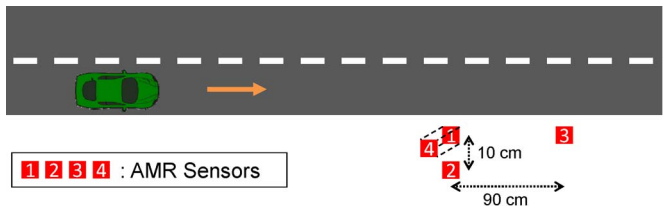

Fig. 3. Sensor configuration for data collection.

Fig. 3 shows the configuration of the sensing system, which includes four three-axis AMR sensors placed on the side of the road. The objective of the system is to count the number of vehicles, measure the speed, and classify the vehicles that pass in the adjacent lane. Sensors 1 and 2 are laterally spaced from each other by 0.1 m. Sensor 3 is placed 0.9 m longitudinally downstream from sensor 1. Sensor 4 is placed 0.3 m vertically above sensor 1. Sensors 1 and 2 are together used to obtain a rough estimate of the lateral location of the vehicle and make the sensing system robust to the traffic in the nonadjacent lane. This method is described in Section IV. Sensors 1 and 3 are together used to calculate the longitudinal speed of the vehicle. The speed estimation algorithm is described in Section V. Sensor 4 is used along with sensor 1 to get a rough estimate of the average vertical magnetic height of passing vehicles. This is used for vehicle classification, which is described in Section VI.

A single printed circuit board (PCB) contains sensors 1 and 2. Two other PCBs contain sensors 3 and 4. The PCBs include Microchip dsPIC microcontrollers, which sample the sensors output at 1 kHz with 12-bit analogue-to-digital converters

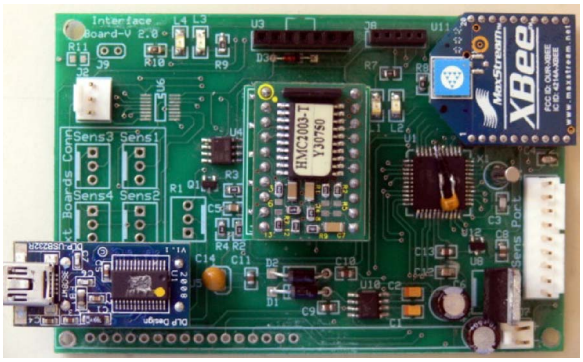

Fig. 4. Developed PCB for data acquisition and wireless transmission.

(ADCs). The magnetic field is read in as arbitrary voltage units (counts) as provided by the ADCs. The data is transferred from the PCBs to a laptop, either wirelessly or through a serial port. The XBee wireless module from Digi is used for wireless communication. This module has an outdoor line-of-sight range of 100 m, required power of 150 mW, and a radio-frequency data rate of 250 kb/s. Fig. 4 shows the developed PCB.

III. Vehicle Detection and Counting

As mentioned in the previous section, the recorded signals from the sensors placed adjacent to the road are more uniform compared to the case that the sensors are on the road. This behavior makes the detection more reliable, because large oscillations in the signals can cause errors due to the double detection of a single vehicle. In particular, it was observed that the signals measured along the z-axis have very similar patterns for a large variety of vehicles. Hence, magnetic readings of the z-axis of sensor 1 are used for detecting and counting the passing vehicles in the adjacent lane. A threshold of 30 counts was used as the vehicle detection threshold. This threshold was experimentally selected. If it is set very high, smaller vehicles will not be detected, and if it is set very low, a higher percentage of vehicles that pass in the nonadjacent lane will be detected. Although a robust algorithm is developed to reduce the false detections due to vehicles that pass in the nonadjacent lane (described in Section IV), it is good to avoid false detections at an early stage to have a minimized final false detection rate. Signals from 188 vehicles driving in the adjacent lane were recorded in two days during afternoon hours, with clear-sky conditions. Out of the 188 vehicles, 186 vehicles created a large-enough signal to be detected, resulting in a detection rate of 99%. Fig. 5 shows a sample signal recorded from a jeep SUV that passes in the adjacent lane, two unknown vehicles that pass in the nonadjacent lane, and a Mazda sedan that passes in the adjacent lane at lateral distances of 2, 5.3, 4.6, and 1.6 m from the sensors, respectively. The lateral distance was measured only for reference purposes by a sonar sensor that faces the road.

IV. Robustness to Traffic on the Nonadjacent Lane

While measuring traffic parameters on the lane adjacent to the sensors, the signals from more than 216 vehicles that pass

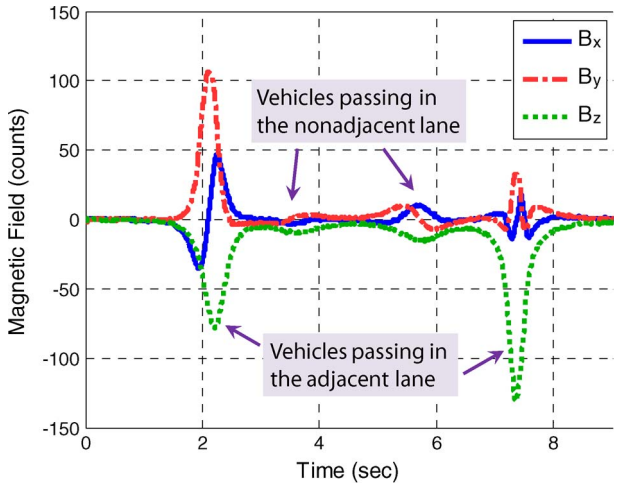

Fig. 5. Recorded magnetic field from a jeep SUV and a Mazda sedan that pass in the adjacent lane and two other vehicles that pass in the nonadjacent lane.

in the nonadjacent lane (the lane next to the closest lane to the sensors) were also recorded. Analyzing the data, it was observed that passenger sedans, SUVs, and pickups that travel in the nonadjacent lane typically do not create errors in the sensing system signals. However, larger vehicles (e.g., trucks and buses) that pass in the nonadjacent lane may create large enough signals to cause false detections and affect the accuracy of the system. The false detections can significantly increase the detection error. In our experiments, 15 out of 216 vehicles created a large-enough signal to be miscounted as vehicles that pass in the adjacent lane. If uncorrected, this will cause an overdetection error of 8%. The results presented in [12] show a similar error rate from the false detection of vehicles in the adjacent lanes, ranging from 5.6% to 15.4% in different weather conditions, even when the AMR sensors are embedded in the middle of the lane in the road. Note that increasing the detection threshold is not an effective solution to address this problem. Although it may reduce the number of false calls, it will also increase the number of missed calls due to smaller vehicles not being detected because of the higher threshold, as experienced in [13]. To correct for vehicle detection errors that can occur due to vehicles in the nonadjacent lane, the following method is proposed.

It is shown through analytical modeling and experimental measurements that the magnetic field intensity around a vehicle has a relation that approximately varies as $1/x$ with distance, where x is the lateral distance from the vehicle [14]. Using sensor 2, an estimate of the lateral distance of the vehicle can be obtained by simply evaluating the ratio of the maximum of the measured magnetic fields between sensors 2 and 1 B_2/B_1. As the distance x increases, the two sensors read roughly the same magnetic field intensity. The closer the ratio of magnetic fields is to 1, the larger the lateral distance becomes. In addition, the vehicles that pass in the nonadjacent lane have a much lower peak value $B_{\max}$, on the average, compared to vehicles that pass in the adjacent lane. These two metrics can be used to reject the traffic passing in the nonadjacent lane, which affects the sensors. Fig. 6 shows the result of applying the proposed method to the data set. A support vector machine has been

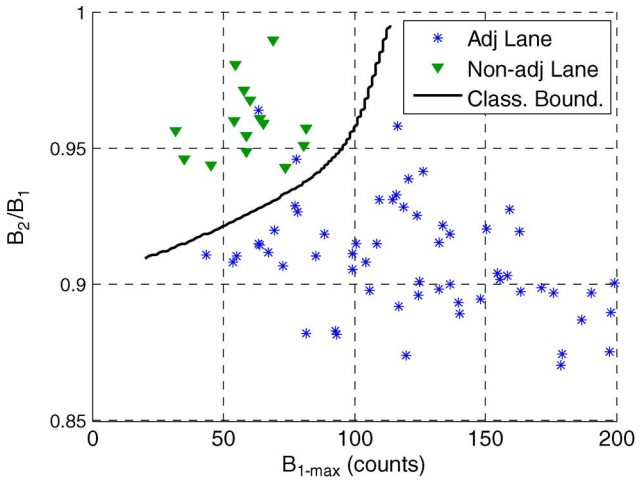

Fig. 6. Use of the ratio B_2/B_1 and $B_{1-\max}$ to reject the traffic in the nonadjacent lane.

used to come up with a classification boundary [15]. Using the proposed method, the error reduces from 8% to 1%. Based on the data of 216 vehicles shown in Fig. 6, it is shown that the proposed classification boundary accurately classifies 99% of the vehicles as correctly being in the adjacent or nonadjacent lane. All of the nonadjacent vehicles are correctly rejected. Only 2 of the 201 adjacent lane vehicles are incorrectly classified as nonadjacent.

V. Speed Estimation

Speed estimation of a passing vehicle is required to measure the vehicle length, which is used for vehicle classification. Speed estimation also has other applications; for example, it has been used by researchers to estimate the queue length for ramp-metering algorithms [16]. Transportation agencies use estimated speed information for setting speed limits and timing traffic signals [17]. There are some proposed methods in the literature for speed measurement using a single magnetic sensor [6]; however, those methods provide only an average estimate of the speed over a number of passing vehicles. To measure individual vehicle speed, two longitudinally spaced sensors are required. The conventional method for estimating speed with two magnetic sensors is based on the detection times of the two sensors. If the detection times for sensors "a" and "b" are $t_{a,ON}$, $t_{a,OFF}$, $t_{b,ON}$, and $t_{b,OFF}$, an estimate of the speed can be calculated as

$$v = \frac{d_{a-b}}{\left((t_{b,ON} - t_{a,ON}) + (t_{b,OFF} - t_{a,OFF})\right)/2} \qquad (1)$$

where d_{a-b} is the distance between sensors "a" and "b", and $t_{a,ON}$ and $t_{b,ON}$ are the timestamps that the sensor signal goes over the detection threshold, for sensors "a" and "b", respectively. $t_{a,OFF}$ and $t_{b,OFF}$ are the timestamps that the sensor signal drops below the detection threshold for sensors "a" and "b", respectively. One of the primary factors that affect the accuracy of the speed estimates is the distance between the sensors; more accurate estimates are obtained by placing sensors farther away from each other. For example, [18] recommends a separation of 4.9 m for speed estimation using two inductive loops. As another example, [19] recommends a separation of 3.1–3.7 m (10–12 ft) between the sensors for arterial applications and 6.1–7.3 m (20–24 ft) for freeway applications. However, none of the aforementioned references specify what the accuracy of the estimates will be. On the other hand, the problem with a large distance between the sensors is that a vehicle may perform a maneuver that may only be detected by one sensor [17]. This phenomenon will affect the synchronization between the sensors, which is required for speed estimation. Note that another factor in the accuracy of the estimated speed is SNR; the higher the SNR is, the more accurate the estimates become. As mentioned in the previous section, signals of lower level are obtained when placing the sensors on the side of the road compared to the case that the sensors are placed on the surface of the road, in the middle of the lane, and hence, the sensors outputs are amplified to get a higher SNR.

In [17], a method for speed estimation is proposed based on signals from two ILDs that are separated by a distance of 6 m using detection times. Their method detects and drops the data points from "irregular driving vehicles," defined as vehicles that do not perfectly travel in parallel with the line that connects the center of the sensors. After dropping these data points, the maximum absolute value of the errors was within 5%. However, in their experiments, more than 8% of the detected vehicles were categorized as "irregular driving vehicles," and hence, their speed was not estimated. This situation is not favorable for vehicle classification based on the magnetic length of passing vehicles.

In [20], a method for the estimation of speed is proposed, which is based on using three magnetic sensor nodes. The accuracy of the method is measured by driving a vehicle at a constant speed of 5.5 m/s (12 mi/h) over the sensors multiple times. The reported estimation error varies in the range of 5%–20%, underestimating the actual speed in all cases.

In [21], another method for speed estimation is proposed, which is based on using four magnetic sensors nodes: two nodes are placed on one side, and two nodes are placed on the other side of a one-lane road. The distance between the nodes on each side is 6 m. The results of the speed estimation method show maximum errors of 13%, with test speeds ranging from 6 m/s to 13 m/s (13.4–29 mi/h).

The goal of the proposed system in this paper is to reduce the distance between the sensors to a minimum and still achieve highly accurate speed estimates by using sophisticated signal processing techniques to measure the time delay. In the designed system, the speed of each passing vehicle is determined by measuring the time delay between the signals of the two magnetic sensors placed longitudinally apart, sensors 1 and 3. The delay is calculated by taking the cross correlation between the signals of the two sensors and then finding the time delay by looking at the value where the resulting signal from the cross correlation is maximized. Knowing the time delay and the distance between the two sensors, the speed of the passing vehicle is estimated. This algorithm is described in the following section.

A. Speed Estimation Algorithm

Consider the magnitude of the magnetic field signals from sensors 1 and 3, B_{1mag} and B_{3mag}, respectively. We expect that B_{3mag} will have the same shape as B_{1mag} but will be shifted in time, because sensor 3 is longitudinally spaced apart from sensor 1, downstream with respect to the vehicle. Ideally, the delay in time between the signal waveforms will have the following relation with the speed of the passing vehicle v:

$$\delta t = \frac{d_{13}}{v} \tag{2}$$

where d_{13} is the distance between sensors 1 and 3, and δt is the time delay between the sensors signals to be calculated. Denoting the sampling time by T_s, B_{3mag} should be delayed by $n_d = \delta t/T_s$ samples with respect to B_{1mag}. One reliable method of calculating the time delay is by using the cross correlation between the two signals. The time delay in terms of samples is given by

$$n_d = \arg\max_n f[n] \tag{3}$$

where

$$f[n] = \sum_{m=0}^{N-1} B_{1mag}[m]B_{3mag}[m-n] \;\&\; -(N-1) \le n \le N-1 \tag{4}$$

and N is the total number of samples for which the cross correlation is being computed. This computation is on the order of N^2 calculations [22]. The discrete Fourier transform (DFT) can be adopted to compute $f[n]$, which results in a significantly less number of required calculations. The method is described in the following paragraphs. Define

$$\begin{aligned} z_1[n] &= B_{1mag}[n] \;\&\; z_2[n] = B_{3mag}\left[(N-1)-n\right] \\ &\qquad 0 \le n \le N-1 \\ g[n] &= f\left[n-(N-1)\right] \quad 0 \le n \le 2N-2. \end{aligned} \tag{5}$$

It is shown that $z_2[n]$ is simply the flipped version of $B_{3mag}[n]$ and $g[n]$ is the shifted version of $f[n]$. Now, we rewrite (3) in terms of $g[n]$ as

$$n_d = \arg\max_n f[n] = \left(\arg\max_n g[n]\right) - (N-1). \tag{6}$$

We can also write $g[n]$ as follows:

$$\begin{aligned} g[n] &= f\left[n-(N-1)\right] \\ &= \sum_{m=0}^{N-1} B_{1mag}[m]B_{3mag}\left[m-(n-(N-1))\right] \\ &= \sum_{m=0}^{N-1} B_{1mag}[m]B_{3mag}\left[(N-1)-(n-m)\right] \\ &= \sum_{m=0}^{N-1} z_1[m]z_2[n-m] = z_1[n] * z_2[n]. \end{aligned} \tag{7}$$

Therefore, we have written $g[n]$ in terms of the linear convolution of $z_1[n]$ and $z_2[n]$. The next step is to calculate this convolution in an efficient way. Based on the properties of the DFT [22], [23], we know that

$$\begin{aligned} x_3[n] &= \sum_{m=0}^{N-1} x_1[m]x_2\left[(n-m) mod\, N\right] = x_1[n] \circledast x_2[n] \\ &\Leftrightarrow X_3[k] = X_1[k]X_2[k] \\ &\qquad 0 \le n, \quad k \le N-1 \end{aligned} \tag{8}$$

where $\circledast$ denotes the circular convolution, and $X[k]$ is the DFT of $x[n]$, or

$$X[k] = DFT\left(x[n]\right) = \sum_{m=0}^{N-1} x[m]e^{-j\left(\frac{2\pi kn}{N}\right)} \qquad 0 \le k \le N-1. \tag{9}$$

In general, a circular convolution differs from a linear convolution. In a circular convolution, the second sequence is "circularly" shifted with respect to the first sequence. However, we can use the relation in (8) to obtain $g[n]$ if we pad the original signals $z_1[n]$ and $z_2[n]$ with zeros to a length equal to or greater than the expected length of the linear convolution $(2N-1)$ [22], [23]. Thus, if we define

$$\begin{aligned} \tilde{z}_1[n] &= \begin{cases} z_1[n] & 0 \le n \le N-1 \\ 0 & N \le n \le 2N-1 \end{cases} \\ \tilde{z}_2[n] &= \begin{cases} z_2[n] & 0 \le n \le N-1 \\ 0 & N \le n \le 2N-1 \end{cases} \end{aligned} \tag{10}$$

we have

$$g[n] = IDFT\left(DFT\left(\tilde{z}_1[n]\right) DFT\left(\tilde{z}_2[n]\right)\right). \tag{11}$$

Now that we have calculated $g[n]$, we can obtain n_d based on (6) and calculate the speed based on (2). Note that using fast Fourier transform and inverse fast Fourier transform algorithms for the calculation of DFT and inverse discrete Fourier transform (IDFT), we can calculate $g[n]$ with computational complexity on the order of $N \log N$ compared to the original order of N^2 [22]. As an example, if we originally have $N = 10\,000$ datapoints (10 s of data sampled at 1 kHz), we will have orders of 10^8 and 10^5 for the original and DFT methods, respectively. This difference can be considerable when the system is implemented in a processor for real-time classification.

The main benefit of using the conventional method of finding the difference between the detection times to estimate the speed is its simplicity, which allows for the design of a sensing system with less complexity and reduced power consumption. These requirements are helpful in increasing the battery life of the sensors when the sensors are embedded in the pavement. However, with the sensors on the side of the road, the power can be provided by larger capacity batteries, power lines, solar cells, or a combination of these. Hence, it is possible to utilize more computational power and develop much more accurate algorithms to achieve better performance in speed estimation and consequently achieve better performance in vehicle classification.

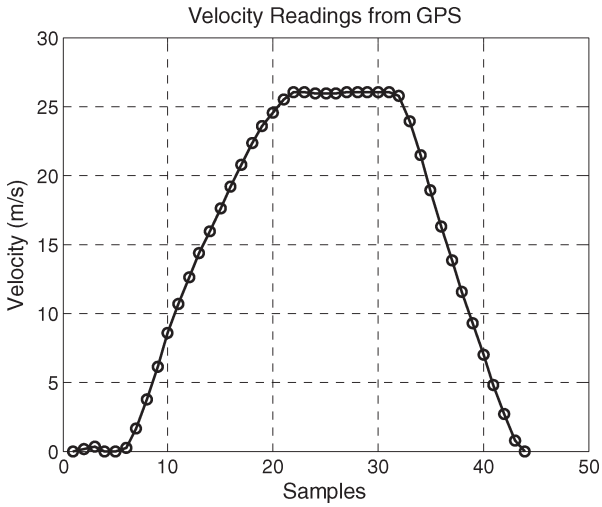

Fig. 7. Speed measurements of the GPS.

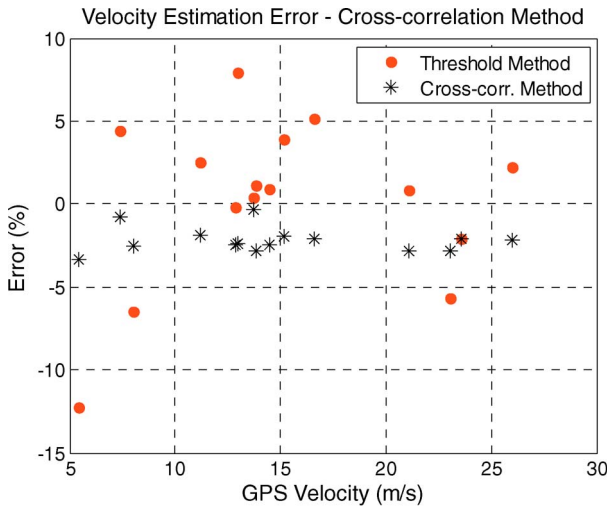

Fig. 8. Speed estimation error using the conventional and cross-correlation methods.

B. Speed Estimation Experimental Results

To check the speed estimation accuracy of the sensing system, the following experiment was conducted at the Minnesota Road Research Facility (MnROAD). The sensing system was placed adjacent to the lane, as shown in Fig. 3. A carrier-phase Global Positioning System (GPS), GPS18 LVC, was mounted on a test vehicle, and its data were captured using a laptop inside the vehicle. The accuracy of the GPS is 0.05 m/s, and its update rate is 1 Hz. A separate data acquisition system was used to capture the roadside sensor data, as shown in the previous experiments.

For each test, the driver started at a long distance away from the sensors, reached the desired speed, passed in front of the sensors with constant speed, and later stopped. One sample of the speed plot that was obtained from the GPS during one test is shown in Fig. 7.

Because the speed is almost constant during the time the vehicle passes in front of the sensors, it is possible to take the average of several data points before the vehicle decelerates and use it as the reference speed that was obtained from the GPS. In all the experiments, 11 satellites were in view for the GPS. The test vehicle was also equipped with a cruise control system, which was used for velocities above ∼13 m/s (30 mi/h) to achieve a more consistent speed.

The error in speed estimates can be calculated as follows:

$$Error = 100\frac{v_{GPS} - v_{est}}{v_{GPS}} \tag{12}$$

where v_{GPS} is the reference GPS speed, and v_{est} is the estimated speed from the magnetic sensors.

Fig. 8 shows the estimation error between the GPS measurement and the sensor estimates when the sensor-based speed was calculated using the simple difference in the detection times described by (1). As shown in Fig. 8, the maximum error for speed estimation is more than 12%. As a result, the magnetic length estimates, being used for vehicle classification, have the same percentage error, because speed estimate errors directly propagate to magnetic length estimate errors. Fig. 8 also shows the estimation error when the cross-correlation method has been applied for speed estimation.

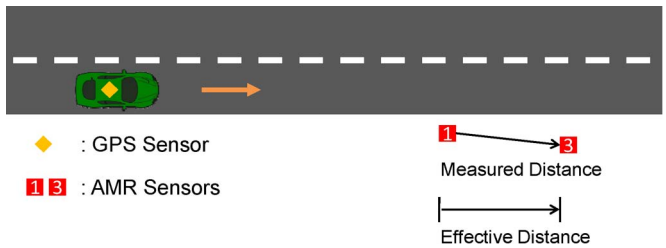

Fig. 9. Sensor configuration for data collection.

As shown in Fig. 8, comparing the conventional and cross-correlation methods, the error range has been reduced from 12% to only 3.5%. Considering the errors of the proposed method, a negative offset is observed, which means that the estimated speed is overestimating the actual speed. This overestimation of speed is because the sensors are not perfectly aligned with the side of the road, as shown in Fig. 9, which makes the actual measured distance between the sensors larger than the effective distance between the sensors.

Multiplying the measured distance between the sensors in this test by a constant factor of 0.98, we get an almost zero-bias speed estimation error distribution, as shown in Fig. 10.

In a general test where there is no reference value for speed calibration, we can use the following algorithm to automatically compensate for misalignment problems.

Assume that sensors 1 and 3 are perfectly aligned with the side of the road and a vehicle passes precisely parallel to the sensors. Therefore, the signal readings of sensors 1 and 3 should be exactly identical, except for a delay that is used for speed estimation. Now, assume that the sensors are not perfectly aligned. In this case, the signal levels at the two sensors will slightly be different. For example, in the scenario depicted in Fig. 9, where sensor 1 is closer to the road than sensor 3, we expect to see slightly higher signal levels for sensor 1 than sensor 3. We can use this difference and partially adjust for the

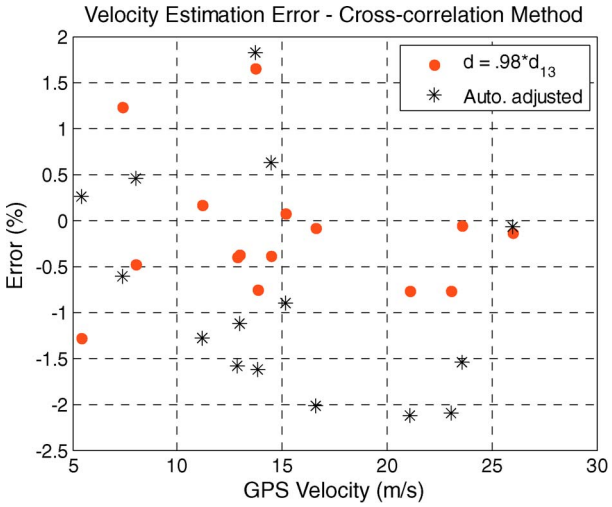

Fig. 10. Speed estimation error. The offset is automatically adjusted.

misalignment. The method is described as follows and is based on using the ratio of integrated values of the two signals. Define

$$B_{int-j} = \int_{t_{j,1}}^{t_{j,2}} B_j dt \qquad j = 1, 3 \tag{13}$$

where $t_{j,1}$ and $t_{j,2}$ are the detection times. Now, defining

$$c = \min\left(\frac{B_{int-1}}{B_{int-3}}, \frac{B_{int-3}}{B_{int-1}}\right) \tag{14}$$

we modify d_{13} as

$$d_{13-corrected} = c * d_{13} \tag{15}$$

and estimate the speed as

$$v = \frac{d_{13-corrected}}{\delta t} \tag{16}$$

where δt is the time difference between the signals calculated earlier. The result of this method is shown in Fig. 10. It is shown that, using this method, we can get an almost-zero-bias error (the mean error is -0.78%) distribution of speed estimations.

As shown in Fig. 10, the maximum error in speed estimation is less than 2.5% over the entire range of speeds, 5–27 m/s (11–60 mi/h).

VI. Vehicle Classification

Vehicle classification is useful in a number of applications, including road maintenance and management, roadway design, emissions evaluation, multimode traffic model development, traffic control, traffic signal design, and toll systems development. For example, the distribution of passing vehicles on a road is used in the estimation of pavement life cycle [24]. There are different vehicle classification methods proposed in the literature based on inductive loops and vision systems. In general, the main drawbacks of using inductive loops are the high cost, the long installation process, and the intrusive nature of sensor installation. The main drawback of systems based on vision is the high sensitivity to weather conditions, as mentioned in Section I. The benefit of using magnetic sensors for vehicle detection is that they are less expensive, more robust to weather conditions, and easier to install. In addition to these benefits, the sensing system proposed in this paper is portable and can be placed adjacent to the road, and therefore, it is not necessary to stop the traffic.

There are existing methods in the literature for vehicle classification based on magnetic sensors. However, the main limitation of these methods is the poor performance in differentiating sedans versus SUVs, pickups, and vans; hence, these two classes are usually combined, as shown in [9] and [10], or only vans are classified as a separate class [8], [11], [25].

In [6], a vehicle classification method is proposed based on the hill pattern of magnetic signatures that were obtained from a single magnetic sensor. Vehicles are classified into seven classes, including sedans, SUVs, and vans. However, the classification accuracy that has been achieved is only 63%.

A classification method based on the average bar and hill pattern recognition schemes is proposed in [26]. Vehicles are classified into four classes, including sedans and SUVs/vans. About 95% of the vehicles are correctly classified; however, the number of SUVs/vans in the data set is only 5% of the total vehicles compared to the total number of sedans, which is 84%.

The classification method proposed in this section is based on using the magnetic length and an estimate of the average vertical height of the passing vehicles. Vehicles are classified into the following four classes.

- Class I: Sedans.
- Class II: SUVs, pickups, and vans.
- Class III: Buses, two- and three-axle trucks.
- Class IV: Articulated buses and four- to six-axle trucks.

Section V described how the speed of each passing vehicle was calculated. In addition, the time duration for which the passing vehicle's magnetic field stays above a detection threshold can be measured to calculate occupancy. The product of the vehicle's estimated speed and the time duration (occupancy) provides the vehicle's magnetic length. Note that the vehicle's magnetic length can slightly be different from its actual physical length. This is because the vehicle magnetic field extends beyond its physical boundaries. However, the length can be calculated with sufficient accuracy for vehicle classification. Of the three axes signals, the magnetic signals along the z-axis were observed to have a very consistent pattern for different types of vehicles. Therefore, magnetic readings of the z-axis were used for measuring the magnetic length, and a threshold of 30 counts was used for the vehicle detection duration measurement. Examples of magnetic signatures are provided in the Appendix.

Fig. 11 shows the measured magnetic length for various vehicles in four classes. As shown in this figure, the magnetic lengths of vehicles in classes III and IV are clearly distinguishable from those of vehicles in classes I and II. As a result, by using only this single feature, it is possible to accurately classify vehicles in these two classes. This is expected, because the actual lengths of the vehicles in classes I and II and vehicles in classes III and IV are very different. However, because vehicles in classes I and II have similar lengths and, consequently, similar magnetic lengths, it is not possible to classify them only

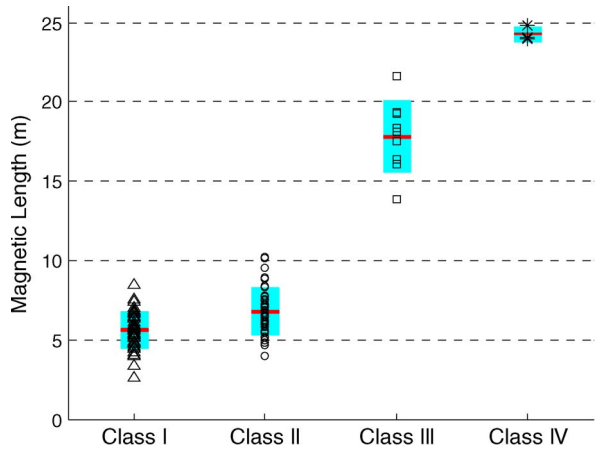

Fig. 11. Magnetic length and classification for various types of vehicles.

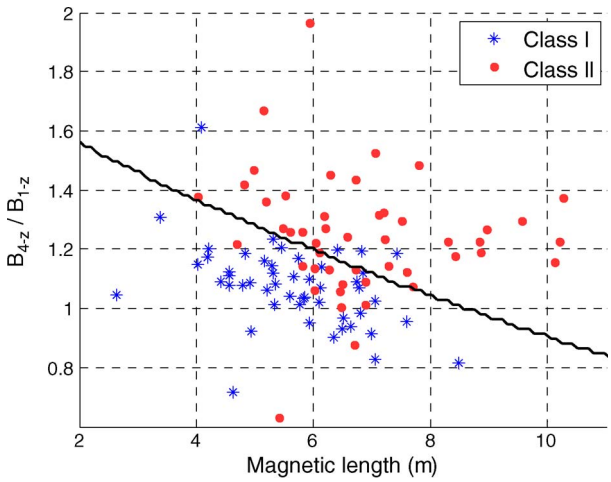

Fig. 12. Classifying class-I and class-II vehicles.

by magnetic length. To improve the classification of vehicles between classes I and II, the following additional signal processing is adopted.

It is expected that higher vertical locations of magnetic components in a vehicle in class II lead to a higher magnetic height compared to vehicles in class I. Placing another sensor, sensor 4, about 0.25 m vertically above sensor 1, it is expected that the ratio B_{4-z}/B_{1-z} will distinctly be larger for vehicles in class II. This ratio, along with the magnetic length, can be used to create more separable boundaries to classify between class-I and class-II vehicles. The result is shown in Fig. 12, where a support vector machine has been used to come up with a classification boundary [15]. Using these two features, 83% of the vehicles are correctly classified into classes I and II. Note that the two features proposed for classification are very easy to implement and are based on the physical magnetic properties of vehicles and not based on some heuristic features and methods such as hill patterns or neural networks.

VII. Right-Turn Detection

The objective of the system described in this section is to count the number of right turns versus the number of straight-driving vehicles at a traffic intersection. This portable system

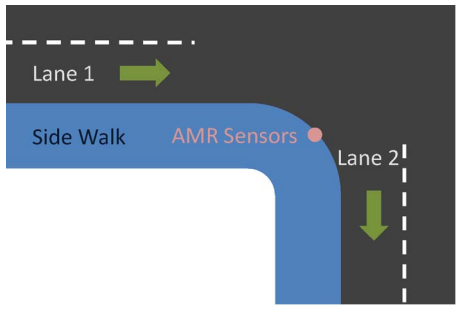

Fig. 13. Right-turn detection and placement of the AMR sensors.

can be used to count the number of right turns at an intersection, replacing the current method, which is based on manual counting. This information can be used for adjusting the traffic lights. The sensors are placed at an intersection, as shown in Fig. 13.

Our objective is to determine the percentage of the vehicles that move in lane 1 and make a right turn to lane 2. Recall that, for traffic measurement, when vehicles travel in a straight line, the magnetic sensors could be placed on the side of the road, and vehicles should typically pass within a distance of 2.5 m from the sensors to be detected. However, when the sensors are placed at the corner of an intersection, half of the turning radius (∼2–3 m) is added to the lateral distance from the passing vehicles in lane 1 to the sensors. Thus, most of the vehicles that pass straight in front of the sensors in lane 1 or 2 are not typically detected. The vehicles that are being detected are the vehicles that make a right turn or larger vehicles that move straight on lane 1 or 2.

By placing one magnetic sensor at the corner side of the road, as shown in Fig. 13, the number of right turns at an intersection can be counted. During the experiments, 56 out of 59 right turns were correctly counted, resulting in a detection rate of 95%. As aforementioned, typically, straight-driving vehicles are not detected, because they pass at a larger distance from the sensor compared to vehicles that make a right turn. However, larger straight-driving vehicles can create large enough signals to be miscounted as vehicles that make right turns. During the experiments, 18 straight-driving vehicles created large enough signals to be miscounted as vehicles that make a right turn, which results in a detection error of 31%.

Two methods, A and B, are proposed to identify and reject the errors caused by straight-driving vehicles, using two and four magnetic sensors, respectively. Considering the sensor configuration shown in Fig. 14, in method A, signals from magnetic sensors 2 and 3 are used. In method B, signals from all the four magnetic sensors are used. The two methods are presented in the following sections. Note that the sensor configuration used for right-turn detection, as shown in Fig. 14, is different from the sensor configuration shown in Fig. 3.

A. Method A

As mentioned in Section III, it can be shown through both analytical modeling and experimental measurements that the magnetic field intensity around a vehicle has a relation that approximately varies as $1/x$ with distance, where x is the lateral

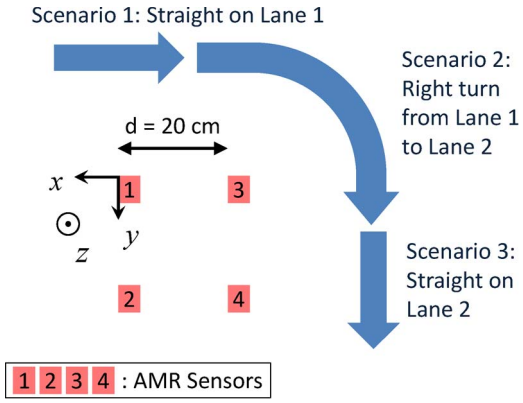

Fig. 14. Magnetic-sensor configuration for the right-turn detection system.

distance from the vehicle [14]. This phenomenon is used in that case to reject the traffic in the nonadjacent lane, which creates large enough signals to affect the sensors. In a right-turn detection system, generally, the traffic going straight in lanes 1 and 2 will pass at a larger lateral distance from the sensors than a vehicle that makes a right turn. Hence, for magnetic sensors 2 and 3, we expect that the ratio $r = B_{max-2}/B_{max-3}$ is closer to 1 during scenarios 1 and 3 compared to scenario 2, as shown in Fig. 14.

B. Method B

Using all the information from all the four magnetic sensors, the following is expected when integrating the signals of each detected vehicle:

$$\text{Scenario 1}: \quad B_{int-1} \cong B_{int-3} > B_{int-2} \cong B_{int-4} \tag{17}$$

$$\text{Scenario 2}: \quad B_{int-3} > B_{int-1} \cong B_{int-4} > B_{int-2} \tag{18}$$

$$\text{Scenario 3}: \quad B_{int-3} \cong B_{int-4} > B_{int-1} \cong B_{int-2}. \tag{19}$$

Now, consider four points in a 3-D space located at $(0, 0, int_{B1})$, $(0, d, int_{B2})$, $(-d, 0, int_{B3})$, and $(-d, d, int_{B4})$, where x and y of each point show the position of a magnetic sensor with respect to the origin (sensor 1), and z shows the value of B_{int-i} for each sensor. Next, we fit a plane with a normal vector $\hat{n}$ to these four points and define $\hat{n}_p$ as the projection of $\hat{n}$ into the xy plane and γ as the angle between $\hat{n}_p$ and the x-axis. It is expected that, for scenarios 1, 2, and 3, the angle γ will be close to 90°, 45°, and 0°, respectively. The angle γ is calculated as follows. The equation of a plane is

$$\hat{n}.(p - p_0) = 0 \tag{20}$$

where p_0 is the position of a known point on the plane, $\hat{n}$ is a nonzero vector normal to the plane, and p is a point on the plane. Expanding this equation, we get

$$n_x(x-x_0)+n_y(y-y_0)+n_z(z-z_0) = 0 \rightarrow ax + by + c = z \tag{21}$$

where

$$a = -\frac{n_x}{n_z} \quad b = -\frac{n_y}{n_z} \quad c = \frac{n_x x_0 + n_y y_0}{n_z} + z_0.$$

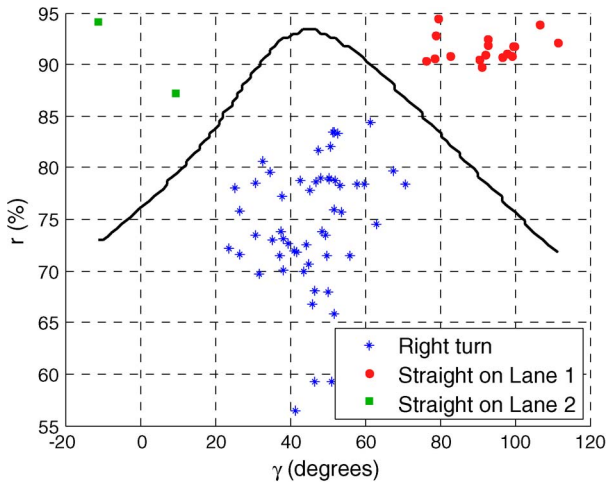

Fig. 15. Results of applying the support vector machine algorithm to obtain classification boundaries.

Hence

$$\gamma = \text{atan}\left(\frac{n_y}{n_x}\right) = \text{atan}\left(\frac{b}{a}\right). \tag{22}$$

Therefore, we should obtain a, b, and c, which can be done using a least squares method, i.e.,

$$y = Hx + v \rightarrow \hat{x} = (H^T H)^{-1} H^T y \tag{23}$$

where

$$x = \begin{bmatrix} a \\ b \\ c \end{bmatrix} \quad H = \begin{bmatrix} 0 & 0 & 1 \\ 0 & d & 1 \\ -d & 0 & 1 \\ -d & d & 1 \end{bmatrix} \quad y = \begin{bmatrix} B_{int-1} \\ B_{int-2} \\ B_{int-3} \\ B_{int-4} \end{bmatrix}$$

and v is the measurement noise.

C. Experimental Results

Methods A and B were applied to the data set obtained from the experiments. The data set was obtained by placing the sensors (with the configuration shown in Fig. 14) at two different intersections and recording signals from passing vehicles. The experiments were performed during noon hours under clear-sky conditions. Fig. 15 shows the results.

As shown in Fig. 15, both methods can be used separately or in combination to reject the straight-driving vehicles, which have created a large-enough signal to be incorrectly detected as a vehicle that makes a right turn. A support vector machine is used to obtain the classification boundaries in Fig. 15 [15]. If only one of the methods is used, the separation between the classes will be smaller, and the measurements will be less separated. These results show that straight-driving vehicles that have created a large-enough signal to be detected by the sensors can completely be excluded, reducing the 31% misdetection error to 0%.

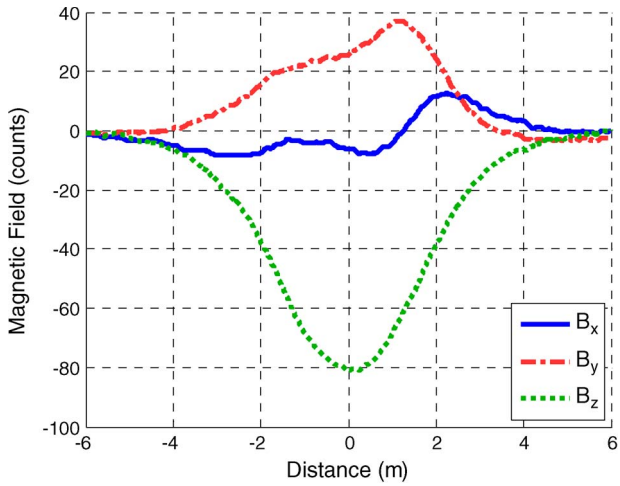

Fig. 16. Magnetic signature of a Nissan Maxima (class I) that passes at 1.6 m from the sensors.

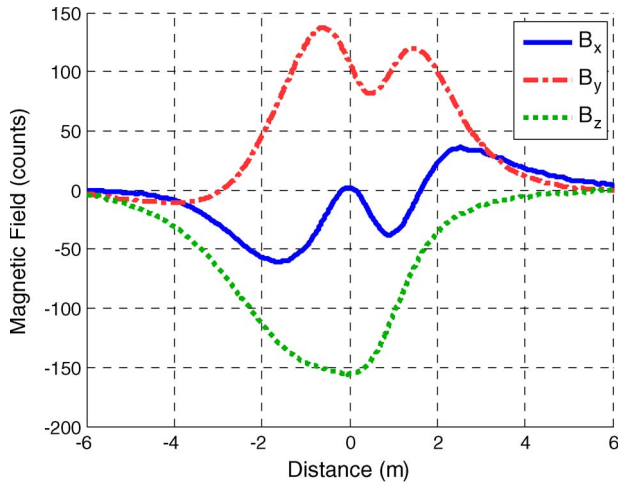

Fig. 17. Magnetic signature of a Toyota Highlander SUV (class II) that passes at 1.4 m from the sensors.

VIII. Conclusion

This paper has proposed a portable and low-cost sensing system based on magnetic sensors that can be placed adjacent to the road and be used for traffic counting, speed measurement, and vehicle classification in the lane adjacent to the sensors. The vehicle classification and speed measurement in this paper are enabled using multiple spatially separated magnetic sensors. Through experimental data from 188 vehicles, it is shown that the traffic counting accuracy of the system is 99%. A method is also proposed to make the system robust to the traffic in the nonadjacent lane. The false calls caused by the traffic in the nonadjacent lane, if uncorrected, can cause an 8% detection error. However, using the proposed method, the error reduces to 1%. Speed estimation is done by placing two magnetic sensors 0.9 m longitudinally apart and taking the cross-correlation between the signals from the two sensors. Digital signal processing methods are adopted to reduce the computation effort. The speed estimation method is verified by mounting a test vehicle with a GPS. Experimental results show a maximum of 2.5% error in speed estimates over the range of 5–27 m/s (11–60 mi/h). Vehicle classification is performed based on the magnetic length and average magnetic height of vehicles. Vehicle length is estimated by multiplying the detection time by the estimated speed. The average vertical magnetic height is estimated using two magnetic sensors that are vertically spaced by about 0.3 m. Finally, it is shown that the sensing system can be used to reliably count the number of right turns at an intersection, with an accuracy of 95%. The challenge in counting the number of right turns is the false calls created by larger straight-driving vehicles, which, if uncorrected, cause 31% overdetection. Two methods are proposed based on using two and four magnetic sensors, which totally eliminate this error.

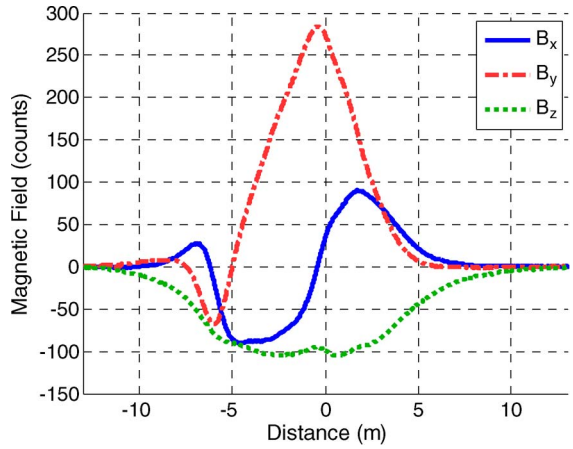

Fig. 18. Magnetic signature of a cement truck (class III) that passes at 1.5 m from the sensors.

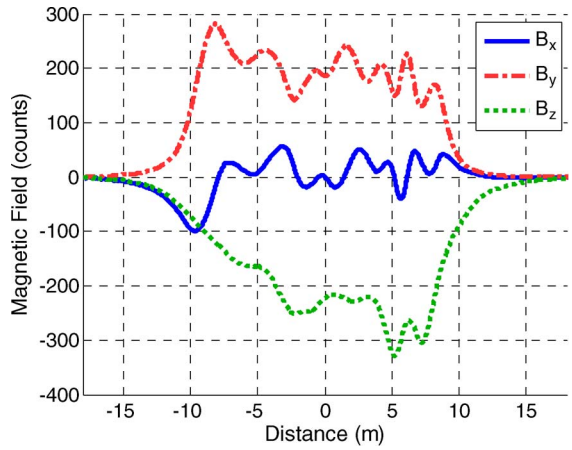

Fig. 19. Magnetic signature of an articulated bus (class IV) that passes at 1.2 m from the sensors.

Appendix

Figs. 16–19 show four examples of magnetic signatures for vehicles in classes I–IV.

References

[1] S. Jeng and S. Ritchie, "Real-time vehicle classification using inductive-loop signature data," *Transp. Res. Rec., J. Transp. Res. Board*, vol. 2086, pp. 8–22, 2008. [Online]. Available: http://dx.doi.org/10.3141/2086-02

[2] S. Gupte, O. Masoud, R. F. K. Martin, and N. P. Papanikolopoulos, "Detection and classification of vehicles," *IEEE Trans. Intell. Transp. Syst.*, vol. 3, no. 1, pp. 37–47, Mar. 2002.

[3] H. Cheng, H. Du, L. Hu, and C. Glazier, "Vehicle detection and classification using model-based and fuzzy logic approaches," *Transp. Res. Rec., J. Transp. Res. Board*, vol. 1935, pp. 154–162, 2005. [Online]. Available: http://dx.doi.org/10.3141/1935-18
[4] J. Medina, M. Chitturi, and R. Benekohal, "Effects of fog, snow, and rain on video detection systems at intersections," *Transp. Lett., Int. J. Transp. Res.*, vol. 2, no. 1, pp. 1–12, Jan. 2010. [Online]. Available: http://dx.doi.org/10.3328/TL.2010.02.01.1-12
[5] M. J. Caruso and L. S. Withanawasam, "Vehicle detection and compass applications using AMR magnetic sensors," in *Sens. Expo Proc.*, 1999, pp. 477–489.
[6] S. Cheung, S. Coleri, B. Dundar, S. Ganesh, C. Tan, and P. Varaiya, "Traffic measurement and vehicle classification with single magnetic sensor," *Transp. Res. Rec., J. Transp. Res. Board*, vol. 1917, pp. 173–181, 2005. [Online]. Available: http://dx.doi.org/10.3141/1917-19
[7] S. Kaewkamnerd, J. Chinrungrueng, R. Pongthornseri, and S. Dumnin, "Vehicle classification based on magnetic sensor signal," in *Proc. IEEE ICIA*, 2010, pp. 935–939.
[8] M. Bottero, B. Dalla Chiara, and F. P. Deflorio, "Wireless sensor networks for traffic monitoring in a logistic center," *Transp. Res.—Part C: Emerg. Technol.*, vol. 26, pp. 99–124, Jan. 2013.
[9] Y. He, Y. Du, and L. Sun, "Vehicle classification method based on single-point magnetic sensor," *Proc. Social Behav. Sci.*, vol. 43, pp. 618–627, 2012.
[10] J. Lan and Y. Shi, "Vehicle detection and recognition based on a MEMS magnetic sensor," in *Proc. 4th IEEE Int. Conf. NEMS*, 2009, pp. 404–408.
[11] Z. Feng and W. Mingzhe, "A new SVM algorithm and AMR sensor based vehicle classification," in *Proc. 2nd ICICTA*, 2009, pp. 421–425.
[12] J. Medina, A. Hajbabaie, and R. Benekohal, "Detection performance of wireless magnetometers at signalized intersection and railroad grade crossing under various weather conditions," *Transp. Res. Rec., J. Transp. Res. Board*, vol. 2259, pp. 233–241, 2011. [Online]. Available: http://dx.doi.org/10.3141/2259-22
[13] F. Ahdi, M. K. Khandani, M. Hamedi, and A. Haghani, "Traffic Data Collection and Anonymous Vehicle Detection Using Wireless Sensor Networks," Univ. Maryland, College Park, MD, USA, 2012.
[14] S. Taghvaeeyan and R. Rajamani, "Use of vehicle magnetic signatures for position estimation," *Appl. Phys. Lett.*, vol. 99, no. 13, pp. 134 101-1–134 101-3, Sep. 2011.
[15] E. Alpaydin, *Introduction to Machine Learning*. Cambridge, MA, USA: MIT Press, 2010.
[16] X. Sun and R. Horowitz, "Set of new traffic-responsive ramp-metering algorithms and microscopic simulation results," *Transp. Res. Rec., J. Transp. Res. Board*, vol. 1959, pp. 9–18, 2006.
[17] Y.-K. Ki and D.-K. Baik, "Model for accurate speed measurement using double-loop detectors," *IEEE Trans. Veh. Technol.*, vol. 55, no. 4, pp. 1094–1101, Jul. 2006.
[18] L. A. Klein, M. K. Mills, and D. R. P. Gibson, *Traffic Detector Handbook: Volume I*. Springfield, VA, USA: Nat. Tech. Inf. Service, 2006.
[19] Anonymous, VSN240 Wireless Flush Mount Sensor Data Sheet Sensys Networks. [Online]. Available: Http://Www.Sensysnetworks.Com, VSN240 Wireless Flush Mount Sensor Data Sheet
[20] D. Nan, T. Guozhen, M. Honglian, L. Mingwen, and S. Yao, "Low-power vehicle speed estimation algorithm based on WSN," in *Proc. 11th IEEE Int. Conf. ITSC*, 2008, pp. 1015–1020.
[21] L. Zhang, R. Wang, and L. Cui, "Real-time traffic monitoring with magnetic sensor networks," *J. Inf. Sci. Eng.*, vol. 27, no. 4, pp. 1473–1486, Jul. 2011.
[22] S. Engelberg, *Digital Signal Processing: An Experimental Approach*. New York, NY, USA: Springer-Verlag, 2008.
[23] A. V. Oppenheim, *Digital Signal Processing*. Englewood Cliffs, NJ, USA: Prentice-Hall, 1975.
[24] C. Sun, "An investigation in the use of inductive-loop signatures for vehicle classification," California PATH Program, Inst. Transp. Studies, Richmond, CA, USA, 2000.
[25] W. Zhang, G. Tan, H. Shi, and M. Lin, "A distributed threshold algorithm for vehicle classification based on binary proximity sensors and intelligent neuron classifier," *J. Inf. Sci. Eng.*, vol. 26, no. 3, pp. 769–783, May 2010.
[26] I. Jolevski, A. Markoski, and R. Pasic, "Smart vehicle sensing and classification node with energy-aware vehicle classification algorithm," in *Proc. 33rd Int. Conf. ITI*, 2011, pp. 409–414.

Saber Taghvaeeyan received the B.S. degree in electrical engineering from the University of Tehran, Tehran, Iran, in 2009. He is currently working toward the Ph.D. degree in mechanical engineering at the University of Minnesota, Twin Cities, Minneapolis, MN, USA.

His research interests include sensors, control systems, and vehicle dynamics.

Mr. Taghvaeeyan is the recipient of the 2013 ITS Minnesota Best Student Paper Award and of the University of Minnesota Doctoral Dissertation Fellowship.

Rajesh Rajamani received the B.Tech. degree from the Indian Institute of Technology, Madras, India, in 1989 and the M.S. and Ph.D. degrees from the University of California, Berkeley, CA, USA, in 1991 and 1993, respectively.

He is currently a Professor of mechanical engineering with the University of Minnesota, Twin Cities, Minneapolis, MN. He has been a coauthor of more than 95 journal papers and is a co-inventor on eight patent applications. He is the author of the popular book *Vehicle Dynamics and Control* (Springer-Verlag). His research interests include sensors and control systems for automotive and biomedical applications.

Dr. Rajamani is a Fellow of the American Society of Mechanical Engineers (ASME). He has served as the Chair of the Technical Committee on Automotive Control of the IEEE Control Systems Society (CSS) and on the editorial boards of the IEEE TRANSACTIONS ON CONTROL SYSTEMS TECHNOLOGY and the IEEE/ASME TRANSACTIONS ON MECHATRONICS. He has received the Faculty Early Career Development (CAREER) Award from the National Science Foundation, the 2001 Outstanding Paper Award from the IEEE TRANSACTIONS ON CONTROL SYSTEMS TECHNOLOGY, the Ralph R. Teetor Educational Award from SAE, and the 2007 O. Hugo Schuck Award from the American Automatic Control Council.